

Preparation and Thermoelectric Properties of Flower-Like Nanoparticles of Ce-Doped Bi₂Te₃

Fang Wu,^{1,*} Wenyu Shi,² and Xing Hu²

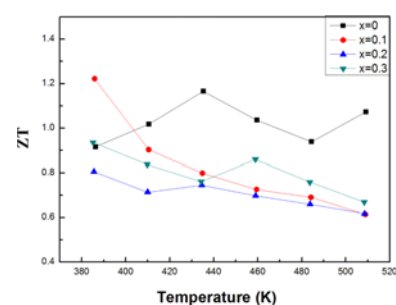
¹School of Physical and Electronic Engineering, Henan Institute of Education, Zhengzhou 450053, China

²School of Physical Engineering and Laboratory of Material Physics, Zhengzhou University, Zhengzhou 450052, China

(received date: 4 May 2014 / accepted date: 2 June 2014 / published date: 10 January 2015)

Ce-doped Ce_xBi_{2-x}Te₃ ($x = 0, 0.1, 0.2, 0.3$) flower-like nanoparticles were synthesized by a hydrothermal method through a careful adjustment of the amount of ethylenediamine tetraacetic acid surfactant. The nanopowders of flower-like nanoparticles were hot-pressed into bulk pellets and the thermoelectric properties of the pellets examined. The results showed that Ce-doping increased the power factor effectively at low temperature; however, the thermal conductivity of the nanopowder too increased because of the lighter atomic mass of Ce compared to Bi. As a result, a ZT value of 1.22, higher than that of the undoped sample, was attained at 386 K for the Ce_{0.1}Bi_{1.9}Te₃ sample.

Keywords: element doping, nanostructure, thermoelectric properties



1. INTRODUCTION

In recent years, thermoelectric (TE) materials have been widely studied for two applications: power generators which convert heat power to electricity and thermoelectric coolers which use electricity to pump heat from one side to the other side against a temperature gradient.^[1,2] TE materials have many advantages, such as environmental friendliness, high reliability and silent operation with no moving parts.^[3-5] The efficiency of a thermoelectric material in the aforementioned applications is determined by the dimensionless figure of merit, defined as $ZT = (S^2 \sigma / \kappa) T$, where S , σ , κ and T are the Seebeck coefficient, electrical conductivity, thermal conductivity, and absolute temperature, respectively. An ideal thermoelectric material exhibits a high ZT value, a large Seebeck coefficient, high electrical conductivity, and low thermal conductivity.^[6,7] In recent years, many methods have been employed to improve the TE properties of materials, of which nanotechnology and energy band engineering are two of the most effective approaches.^[8-10]

The alloys of bismuth telluride, Bi₂Te₃, are some of the best thermoelectric materials operating at approximately room temperature. But the ZT values of the principal

commercial Bi₂Te₃ based alloys have remained around 1 for a long time.^[7] During the past decades, there have been many reports on different attempts to enhance the ZT values of the nanostructured bismuth telluride based alloys. Xie *et al.*^[11] employed the melt spinning method combined with subsequent spark plasma sintering to fabricate nanostructured p -type (Bi,Sb)₂Te₃ samples that exhibit a maximum ZT of 1.5 at about 390 K. Poudel *et al.*^[12] reported that a ZT value of 1.4 at 373 K could be achieved in a p -type nanocrystalline BiSbTe bulk alloy fabricated by ball-milling and subsequent hot-pressing. Cao *et al.*^[13] utilized the hydrothermal method and hot-pressing to prepare nanostructured (Bi,Sb)₂Te₃ bulk samples that demonstrated a high ZT value of 1.28 at 303 K. Compared with the progress reported for p -type Bi₂Te₃-based alloys, the ZT value of n -type Bi₂Te₃ based alloys has not been much improved beyond the value of 1.^[14] Because both p -type and n -type thermoelectric materials are essential for the fabrication of a thermoelectric device, it is very important to optimize the thermoelectric performance of n -type Bi₂Te₃-based alloys.

Based on previous reports, a high ZT may be considered to be related to inhomogeneities on different length scales in the bulk material. So the thermoelectric properties of nanostructured materials should depend on the size and morphology of the microstructural features.^[7] In our previous study,^[15] we synthesized n -type Bi₂Te₃ flower-like nanosheets

*Corresponding author: fwu082@126.com
©KIM and Springer

by the hydrothermal method, and established that a ZT value of 1.16 can be achieved at 423 K with a suitable microstructure. As is known, doping with rare-earth atoms can, in principle, affect the transport properties of thermoelectric materials via three mechanisms: i) by forming enhanced electron states near the Fermi level; ii) by effecting formation of local defects that result in additional carrier scattering; and/or iii) by causing additional carrier scattering due to localized magnetic moments. It is well known that Ce can form resonance electron states near the Fermi level and can strongly affect the electronic transport properties, particularly thermopower.^[16] Therefore, doping flower-like nanosheets of Bi_2Te_3 with rare-earth elements should help improving the TE property of Bi_2Te_3 . However, in our previous study, we found that doping with rare-earth (RE) elements is detrimental to the formation of a flower-like morphology, and that the amount of ethylenediamine tetraacetic acid (EDTA) surfactant used is a key factor in the development of flower-like $\text{RE}_x\text{Bi}_{2-x}\text{Te}_3$ nanoparticles.^[17] In the present paper, we report on the synthesis of $\text{Ce}_x\text{Bi}_{2-x}\text{Te}_3$ ($x=0.1-0.3$) flower-like nanoparticles using the hydrothermal method and investigate the thermoelectric properties of the bulk samples formed from these nanopowders. We found that Ce doping increased the powder factor effectively at a low temperature; we also found that it increased the thermal conductivity as a consequence of its atomic mass being lower than that of Bi. As a result, only at 386 K could the ZT value of the Ce-doped sample attain 1.22, which is higher than that for the undoped sample.

2. EXPERIMENTAL PROCEDURE

The experimental process was similar to that described in our previous work,^[15] except that in the present study, the preparation parameters, mainly the amount of EDTA, were modified for the purpose of obtaining the Ce-doped Bi_2Te_3 flower-like nanoparticles. In brief, analytical-grade (2- x) mmol BiCl_3 , x mmol $\text{Ce}(\text{NO}_3)_3 \cdot 6\text{H}_2\text{O}$ ($x=0, 0.1, 0.2$, and 0.3), and 3 mmol 5N pure Te powder were used as the precursors for the synthesis of $\text{Ce}_x\text{Bi}_{2-x}\text{Te}_3$ nanopowders. The precursors were placed in a Teflon-lined autoclave partially filled with distilled water. Some sodium hydroxide (NaOH) was added as a PH-value controller and a certain amount of EDTA was added as a surfactant. Then, a magnetic stirrer was used to stir the Teflon-lined autoclave for 30 min. Next, 0.35 g NaBH_4 was added to the solution as an organic complex reagent and the autoclave was sealed and kept at 443 K for 24 h. The powders produced were filtered and washed several times using distilled water, dehydrated ethyl alcohol and acetone to remove impurities. Then, the powders were dried in vacuum at 373 K for 6 h and hot-pressed into bulk pellets of diameter 12.5 mm or 15 mm and thickness of about 2 mm at a temperature of 773 K and under a pressure

of 60 MPa in vacuum.

The phases in the powders were investigated by x-ray diffraction (XRD) analysis using Cu-K_α radiation (Rigaku D/MAX-2550p diffractometer, Japan). The data was collected in the 2θ range of $10-80^\circ$ in steps of 0.02° at a scanning speed of $4^\circ/\text{min}$. The morphologies of the powders and bulk pellets were observed by field emission scanning electron microscopy (SEM) (JSM-6700F, Japan). The densities of the bulk pellets were measured by the Archimedes method. The electrical resistivity, ρ , and the Seebeck coefficient, S , of the rectangular bars cut from the $\phi 15$ mm pellets were measured at several temperatures using an LSR-3/800 Seebeck coefficient/Electric Resistance Measuring System (LINSEIS, Germany) under He atmosphere. The thermal conductivity, κ , of the $\phi 12.5$ mm pellets was measured by a thermal diffusivity system (FLASHLINETM 3000, ANTER, USA) using Pyroceram as the reference sample (Provided by ANTER) at several temperature values. The figure of merit, ZT , was calculated from S , ρ and κ of the measured data.

3. RESULTS AND DISCUSSION

Figure 1 shows the x-ray diffraction patterns of the Ce-doped $\text{Ce}_x\text{Bi}_{2-x}\text{Te}_3$ nanopowders prepared with an EDTA amount $\delta=0.23$ g, which is the optimum value we found in our previous work.^[18] As a comparison, undoped Bi_2Te_3 nanopowders prepared with EDTA amount $\delta=0.2$ g mentioned in a previous work were also examined.^[15] It could be seen that for the doping amount $x < 0.3$, all nanopowders displayed a R3m rhombohedral structure similar to that of Bi_2Te_3 , and there were no obvious impurity phases. However, a clear impurity phase could be observed in the $\text{Ce}_{0.3}\text{Bi}_{1.7}\text{Te}_3$ nanopowders. The impurity phase was indexed to Te (from the JCPDS85-0554 card), which indicated that there was an amount of Te present in the $\text{Ce}_{0.3}\text{Bi}_{1.7}\text{Te}_3$ nanopowders. Furthermore, the amount of Ce-

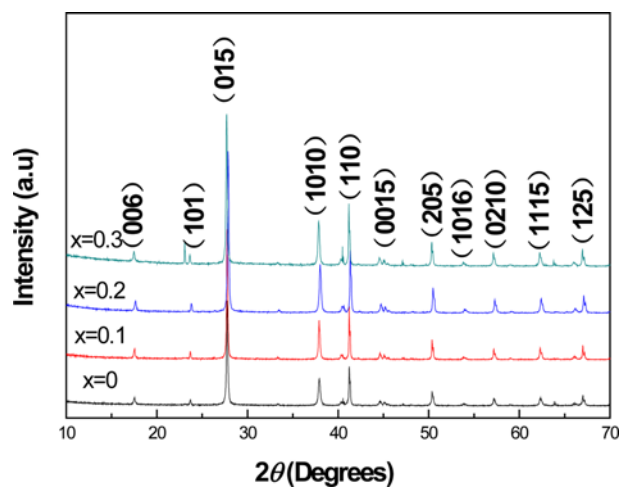


Fig. 1. XRD patterns of $\text{Ce}_x\text{Bi}_{2-x}\text{Te}_3$ nanoparticles.

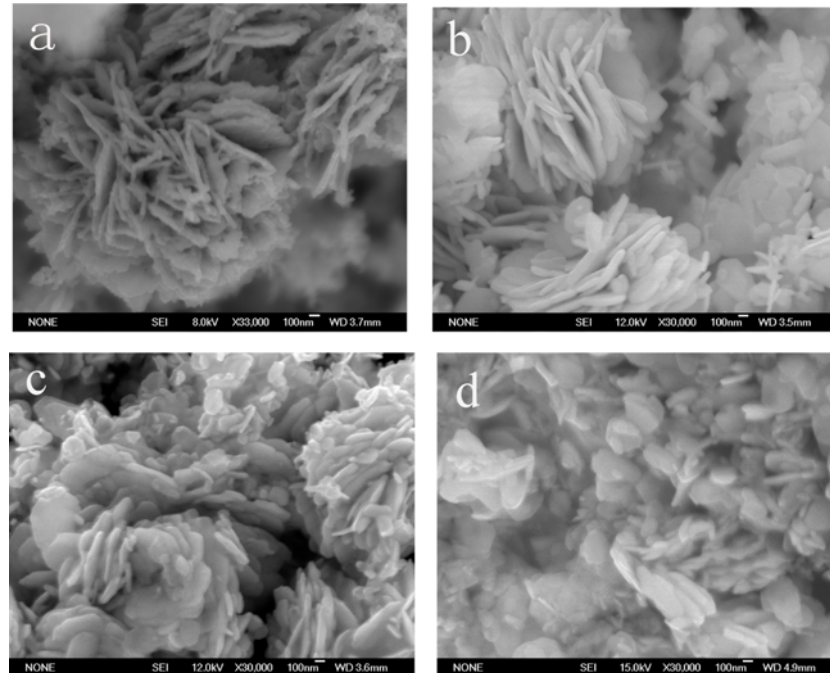


Fig. 2. SEM images of $Ce_xBi_{2-x}Te_3$ powders with different Ce doping amounts (x): (a) $x = 0$, (b) $x = 0.1$, (c) $x = 0.2$, (d) $x = 0.3$.

doping was found to affect the purity of the samples, and the maximum doping amount with which no impurity was observed was $\sim x = 0.2$, as shown in Fig. 1.

Figure 2 demonstrates the morphologies of the $Ce_xBi_{2-x}Te_3$ nanopowders. It can be seen from Fig. 2, for the $x = 0$ and $x = 0.1$ samples, the nanoparticles exhibit flower-like morphologies that are comprised of large sheets of thickness less than 100 nm. For $x = 0.2$, the flower-like morphologies of the nanoparticles was found to be partly destroyed. For the samples with doping higher than $x = 0.3$, the flower-like morphology completely disappeared, and instead flake nanoparticles were observed. This indicates that Ce-doping is not beneficial to the growth of large-sized nanosheets.

As known, the Bi_2Te_3 crystal has a layered hexagonal structure with the Te and Bi atom layers arranged in the order of -Te(1)-Bi-Te(2)-Bi-Te(1)- along the c -axis. Between two Te(1) layers there exist van der Waals bonds, besides which, all remaining bonds are covalent.^[19] When Bi is replaced by Ce or some other rare earth element, the bond strength changes (the proportion of the ionic component of a Ce-Te bond is 21.3% while that for a Bi-Te bond it is only 0.16%^[17]), and therefore the growth rates along the c -axis as well as along the a - and b -axes are affected. In fact, replacing Bi by Ce weakens the bonds in the Te(1)-Bi-Te(2)-Bi-Te(1) layer, but the Van der Waals bonds between two Te(1) layers do not change much. This change in bond strength results in the reduction of the growth rate along the a - and b -axes. This may be the reason why Ce-doping is damaging to the formation of large nanosheets. Referring to our previous

work,^[18] Y-doping is also detrimental to the formation of large sheets because of the same reason, but the flower-like morphologies of Y-doped nanoparticles are superior to those of Ce-doped nanoparticles because the proportion of the ionic component in a Y-Te bond is 17.6%, which is lower than the 21.3% in a Ce-Te bond.

Figure 3 depicts the microstructures of $Ce_xBi_{2-x}Te_3$ bulk samples obtained by hot-pressing the nanopowders. The densities of the samples were 7.1 g/cm^3 , 7.03 g/cm^3 , 7.12 g/cm^3 and 7.30 g/cm^3 for $x = 0, 0.1, 0.2$ and 0.3 respectively, the values being close to the theoretical density of Bi_2Te_3 (7.7 g/cm^3). From Fig. 3, it is evident that the sheet-shaped crystals still remained and that the thickness of the sheets is less than 100 nm; however, the size of the sheets increase significantly along directions parallel to the surface of the sheets because of the hot-pressing at a high temperature. For the samples with $x = 0, 0.1$ and 0.2 , it can also be seen that the microstructure of the hot-pressed bulk pellets prepared from such nanopowders is a mixture of large sheets and small grains, which are desirable factors for the improvement of the TE properties of Bi_2Te_3 -based alloys.^[15] However, for $x = 0.3$, the microstructure is composed of only one large sheet.

Figure 4 demonstrates the electrical resistivity ρ of the $Ce_xBi_{2-x}Te_3$ bulk samples as a function of temperature. As a comparison, the data for the undoped hot-pressed Bi_2Te_3 samples prepared using flower-like nanoparticles as reported in a previous work is also presented.^[15] It can be seen that the ρ of all the samples increased with an increase in

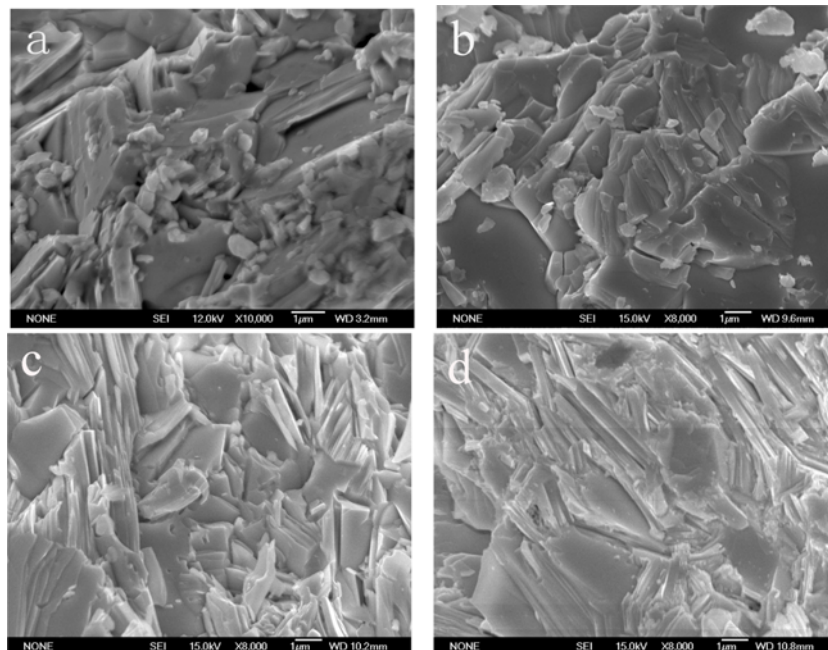


Fig. 3. SEM images of hot-pressed $\text{Ce}_x\text{Bi}_{2-x}\text{Te}_3$ bulk samples with different Ce doping amounts (x): (a) $x = 0$, (b) $x = 0.1$, (c) $x = 0.2$, (d) $x = 0.3$.

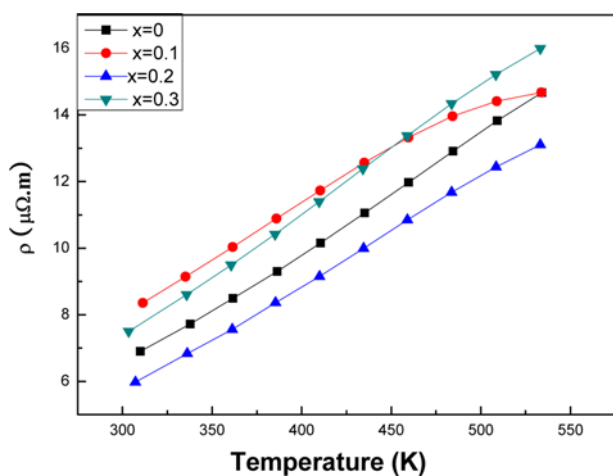


Fig. 4. Electrical resistivity of $\text{Ce}_x\text{Bi}_{2-x}\text{Te}_3$ bulk samples versus temperature.

temperature, exhibiting behavior characteristic of a degenerate semiconductor. In our previous study, we reported that the electrical resistivity of $\text{RE}_{0.2}\text{Bi}_2\text{Te}_3$ ($R = \text{Ce}, \text{Y}, \text{Sm}$) samples doped with rare earth elements is higher than that of the undoped pure Bi_2Te_3 sample, even though it is expected that doping can increase electron concentration.^[17] However, the electrical resistivities of flower-like Ce-doped nanoparticle samples of $\text{Ce}_{0.2}\text{Bi}_{1.8}\text{Te}_3$ are lower than that of the undoped Bi_2Te_3 sample, indicating the advantage such nanopowders offer. The electrical resistivities of $\text{Ce}_{0.1}\text{Bi}_{1.9}\text{Te}_3$ and $\text{Ce}_{0.3}\text{Bi}_{1.7}\text{Te}_3$ too are higher than that of the undoped form. The higher ρ of $\text{Ce}_{0.3}\text{Bi}_{1.7}\text{Te}_3$ can be attributed to the presence of an impurity

phase and the fact that its particles do not possess a flower-like morphology. However, because both $\text{Ce}_{0.1}\text{Bi}_{1.9}\text{Te}_3$ and undoped Bi_2Te_3 samples are prepared from flower-like nanoparticles, it is expected that the ρ of $\text{Ce}_{0.1}\text{Bi}_{1.9}\text{Te}_3$ will be lower than that of the undoped sample. A possible explanation for the ρ of $\text{Ce}_{0.1}\text{Bi}_{1.9}\text{Te}_3$ being higher than that of the undoped form may be as follows. The general expression for the electrical resistivity is^[20]

$$\rho = \frac{1}{\mu n e} = \frac{m^*}{n e^2 \langle \tau \rangle} \quad (1)$$

where μ is the carrier mobility, n carrier concentration, m^* the effective mass of the carrier, e the electron charge, and $\langle \tau \rangle$ is the average relaxation time of the carrier. A lower carrier mobility (corresponding to a shorter $\langle \tau \rangle$) results in a higher electrical resistivity. Ce doping has a two-fold effect on the electrical resistivity. It increases carrier concentration, which is ideal for reducing the electrical resistivity; however, it also intensifies alloy scattering and thus shortens the average relaxation time of the carriers, which is disadvantageous to the reduction of electrical resistivity. Since the $\text{Ce}_{0.1}\text{Bi}_{1.8}\text{Te}_3$ and $\text{Ce}_{0.2}\text{Bi}_{1.8}\text{Te}_3$ both exhibit flower-like nanostructures, the difference in their electrical resistivities can be explained only on the basis of the competition between carrier concentration and alloy scattering. For $\text{Ce}_{0.1}\text{Bi}_{1.9}\text{Te}_3$, the effect of alloy scattering is greater than the effect of the increase in carrier concentration, therefore its electrical resistivity is higher than for the undoped sample. For $\text{Ce}_{0.2}\text{Bi}_{1.8}\text{Te}_3$, the effect of the carrier concentration is larger than the effect of alloy scattering, and therefore, $\text{Ce}_{0.2}\text{Bi}_{1.8}\text{Te}_3$ has a lower elec-

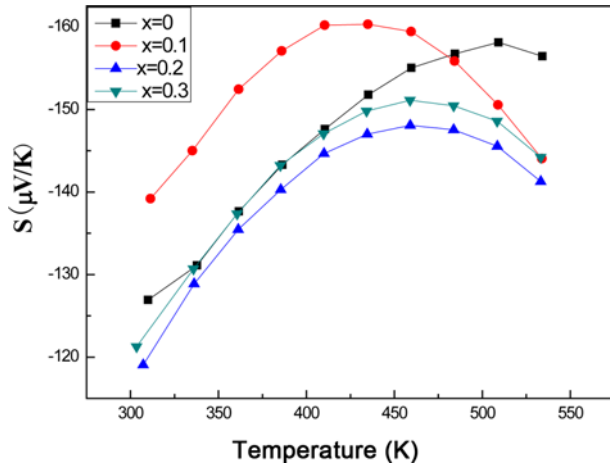


Fig. 5. Seebeck coefficient of $Ce_xBi_{2-x}Te_3$ bulk samples versus temperature.

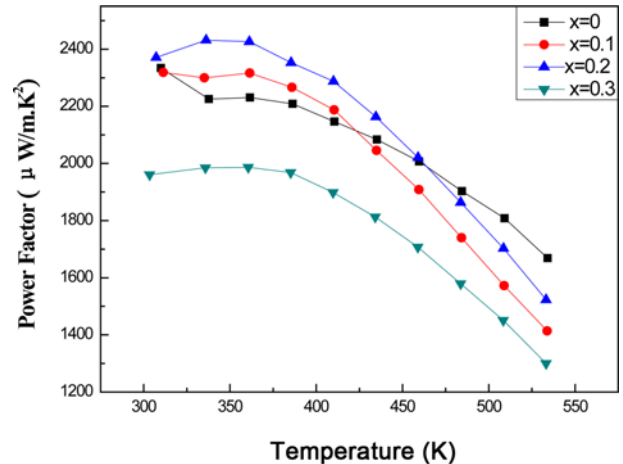


Fig. 6. Power factor of $Ce_xBi_{2-x}Te_3$ bulk samples versus temperature.

trical resistivity than the undoped sample.

Figure 5 shows the Seebeck coefficients of the samples versus temperature. It can be seen that all the samples exhibit n -type conduction as they possess negative Seebeck coefficients in the measured temperature range, indicating that Ce substituting Bi is an example of a donor dopant. From Fig. 4, it can be seen that the electrical resistivity for the $x = 0.1$ sample is higher than those for the $x = 0.2$ and $x = 0.3$ samples, while from Fig. 5 the Seebeck coefficient (absolute value) of the $x = 0.1$ samples is observed to be higher than those for the $x = 0.2$ and $x = 0.3$ samples. This is consistent with our common knowledge of a higher electrical resistivity resulting in a larger Seebeck coefficient. However, the electrical resistivity for the $x = 0.3$ sample was higher than for the undoped sample, as shown in Fig. 4, while from Fig. 5 the Seebeck coefficient (absolute value) of the $x = 0.3$ samples is observed to be lower than that of the undoped sample, possibly because of the impurity phases present in the $Ce_{0.3}Bi_{1.7}Te_3$ sample.

Figure 6 displays the power factor (S^2/ρ) of the samples as a function of temperature. From Fig. 6, it can be seen that below 435 K, the power factors of the $Ce_{0.1}Bi_{1.8}Te_3$ and $Ce_{0.2}Bi_{1.8}Te_3$ samples are higher than that for the undoped sample. This is consistent with Ce forming resonance electron states near the Fermi level and strongly affecting the electronic transport properties, resulting in a higher TE power factor, as mentioned above. This effect may be more evident at lower temperatures. For the $Ce_{0.3}Bi_{1.8}Te_3$ sample, the power factor is lower compared to the undoped sample, mainly due to the impurities in the $Ce_{0.3}Bi_{1.8}Te_3$ sample.

Figure 7 shows the variation in thermal conductivity with temperature. It is expected that Ce-doping introduces a number of point defects into the crystals, which effectively enhance short-wave phonon scattering by reason of atomic mass and strain fluctuations and hence reduce the thermal

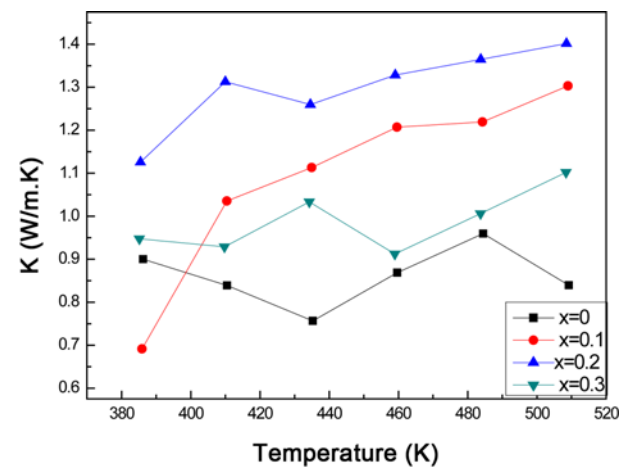


Fig. 7. Thermal conductivity of $Ce_xBi_{2-x}Te_3$ bulk samples versus temperature.

conductivity. However, the thermal conductivities of the $Ce_xBi_{2-x}Te_3$ samples were all higher than for the undoped sample Bi_2Te_3 . Only at 386 K was the thermal conductivity of the $x = 0.1$ sample lower than for the undoped sample. The higher thermal conductivity of $Ce_{0.3}Bi_{1.7}Te_3$ may be attributed to its impure phases, while the reason for the higher thermal conductivities of the $x = 0.1$ and $x = 0.2$ samples may be as a result of the relative atomic mass of the Ce (140.12 g) being less than that of Bi (208.98 g). From Fig. 7 the thermal conductivity of the $Ce_{0.1}Bi_{1.9}Te_3$ is seen to be lower than that for $Ce_{0.2}Bi_{1.8}Te_3$. This may also be related to the above reason. In addition, the difference in the microstructure of the two samples may be another explanation, a phenomenon caused by the superior flower-like morphology of the $Ce_{0.1}Bi_{1.9}Te_3$ nanopowders compared to $Ce_{0.2}Bi_{1.8}Te_3$ nanopowders as shown in Figs. 2(b) and (c).

Figure 8 presents the ZT values of the bulk samples. The ZT value of the optimized doped sample $Ce_{0.1}Bi_{1.9}Te_3$ attains

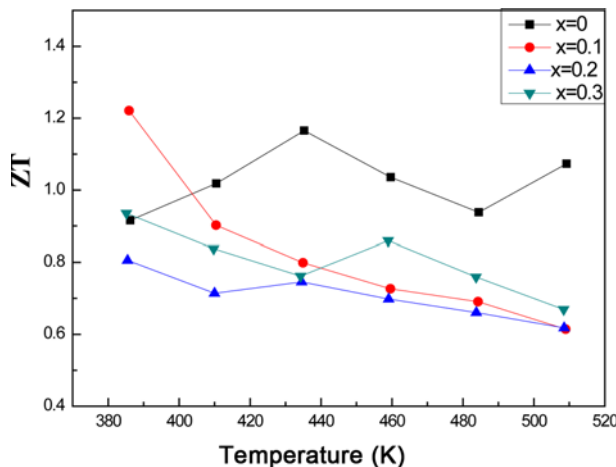


Fig. 8. Figure of merit (ZT) of $Ce_xBi_{2-x}Te_3$ bulk samples versus temperature.

a value of 1.22 at 386 K. As an n -type thermoelectric material, the ZT value of $Ce_{0.1}Bi_{1.9}Te_3$ is relatively high, especially since the ZT value of n -type Bi_2Te_3 -based alloys has until now not been improved much beyond 1.^[14] Only at 386 K was the ZT value of $Ce_{0.1}Bi_{1.9}Te_3$, prepared using flower-like nanoparticles, found to be higher than that for the undoped Bi_2Te_3 bulk sample, also prepared using flower-like nanostructures, owing to the higher thermal conductivity induced by Ce doping.

4. CONCLUSIONS

$Ce_xBi_{2-x}Te_3$ flower-like nanoparticless were synthesized successfully by the hydrothermal method through the control of the amount of EDTA used. We discovered that Ce-doping increased the power factor effectively at low temperature, while also increasing the thermal conductivity because of the lighter atomic mass of the Ce compared to Bi. The cooperation mechanism between the Ce dopant and the flower-like microstructure can result in a relatively high ZT value at 386 K, which is comparable to the highest reported value for n -type Bi_2Te_3 -based alloys.

ACKNOWLEDGEMENTS

This work was supported partly by the Science and Technology Development Program of Henan Province of China (Grant No. 142102210043), the Basic and Advanced

Technology Research Program of Henan Province of China (Grant No. 132300410415), and Key Program of Science and Technology Research of Henan Educational Committee (Grant No. 14A140017).

REFERENCES

1. D. M. Rowe, *CRC Handbook of Thermoelectrics*, p. 1, CRC Press, Boca Raton (1995).
2. T. M. Tritt, *Science* **283**, 804 (1999).
3. X. Gou, H. Xiao, and S. Yang, *Appl. Energ.* **87**, 3131 (2010).
4. C. C. Wang, C. I. Hung, and W. H. Chen, *Energy* **39**, 236 (2012).
5. W. H. Chen, C. Y. Liao, C. I. Hung, and W. L. Huang, *Energy* **45**, 874 (2012).
6. G. J. Snyder and E. S. Toberer, *Nat. Mater.* **7**, 105 (2008).
7. Y. C. Lan, A. J. Minnich, G. Chen, and Z. F. Ren, *Adv. Funct. Mater.* **20**, 357 (2010).
8. M. S. Dresselhaus, G. Chen, M. Y. Tang, R. G. Yang, H. Lee, D. Z. Wang, Z. F. Ren, J. P. Fleurial, and P. Gogna, *Adv. Mater.* **19**, 1043 (2007).
9. G. Q. Zhang, Q. X. Yu, W. Wang, and X. G. Li, *Adv. Mater.* **22**, 1 (2010).
10. Z. G. Chen, G. Han, L. Yang, L. Cheng, and J. Zou, *Prog. Nat. Sci-Mater.* **22**, 535 (2012).
11. W. J. Xie, J. He, H. J. Kang, X. F. Tang, S. Zhu, M. Laver, S. Y. Wang, and J. R. D. Copley, *Nano. Lett.* **10**, 3283 (2010).
12. B. Poudel, Q. Hao, Y. Ma, Y. Lan, A. Minnich, B. Yu, X. Yan, D. Wang, A. Muto, D. Vashaee, X. Chen, J. Liu, M. S. Dresselhaus, G. Chen, and Z. Ren, *Science* **320**, 634 (2008).
13. X. B. Zhao, X. H. Ji, Y. H. Zhang, T. J. Zhu, J. P. Tu, and X. B. Zhang, *Appl. Phys. Lett.* **86**, 062111 (2005).
14. Y. C. Lan, A. J. Minnich, G. Chen, and Z. F. Ren, *Adv. Funct. Mater.* **20**, 357 (2010).
15. F. Wu, H. Z. Song, F. Gao, W. Y. Shi, J. F. Jia, and X. Hu, *J. Electron. Mater.* **42**, 1140 (2013).
16. T. M. Tritt and M. A. Subramanian, *MRS Bull.* **31**, 188 (2006).
17. F. Wu, H. Z. Song, J. F. Jia, and X. Hu, *Prog. Nat. Sci-Mater.* **23**, 408 (2013).
18. W.Y. Shi, F.Wu, K.L. Wang, J.Yang, H.Z. Song, and X. Hu, *J. Electron. Mater.* **43**, 3162 (2014).
19. Q. Zhao and Y. G. Wang, *J. Alloys. Comp.* **497**, 57 (2010).
20. Ö. C. Yelgel and G. P. Srivastava, *J. Appl. Phys.* **113**, 073709 (2013).